Computer Methods and Programs in Biomedicine 255 (2024) 108331

Contents lists available at ScienceDirect

Computer Methods and Programs in Biomedicine

journal homepage: https://www.sciencedirect.com/journal/computer-methods-and-programs-in-biomedicine

An agent-based method to estimate 3D cell migration trajectories from 2D measurements: Quantifying and comparing T vs CAR-T 3D cell migration

Daniel Camacho-Gomez [a,1], Nieves Movilla [a,1], Carlos Borau [a,b], Alejandro Martin [a], Carmen Oñate Salafranca [c], Julian Pardo [c,d], Maria Jose Gomez-Benito [a], Jose Manuel Garcia-Aznar [a,*]

[a] Department of Mechanical Engineering, Multiscale in Mechanical and Biological Engineering (M2BE), Aragon Institute of Engineering Research (I3A), University of Zaragoza, Zaragoza, Spain
[b] Centro Universitario de la Defensa de Zaragoza, Zaragoza, 50090, Spain
[c] Faculty of Medicine, University of Zaragoza/IIS Aragon, Spain
[d] CIBER of Infectious diseases, IS Carlos III, Madrid, Spain

ARTICLE INFO

Keywords:
Microfluidics-based cell cultures
3D cell migration
Agent-based models
Immunotherapy

ABSTRACT

Background and objective:

Immune cell migration is one of the key features that enable immune cells to find invading pathogens, control tissue damage, and eliminate primary developing tumors. Chimeric antigen receptor (CAR) T-cell therapy is a novel strategy in the battle against various cancers. It has been successful in treating hematological tumors, yet it still faces many challenges in the case of solid tumors. In this work, we evaluate the three-dimensional (3D) migration capacity of T and CAR-T cells within dense collagen-based hydrogels. Quantifying three-dimensional (3D) cell migration requires microscopy techniques that may not be readily accessible. Thus, we introduce a straightforward mathematical model designed to infer 3D trajectories of cells from two-dimensional (2D) cell trajectories.

Methods:

We develop a 3D agent-based model (ABM) that simulates the temporal changes in the direction of migration with an inverse transform sampling method. Then, we propose an optimization procedure to accurately orient cell migration over time to reproduce cell migration from 2D experimental cell trajectories. With this model, we simulate cell migration assays of T and CAR-T cells in microfluidic devices conducted under hydrogels with different concentrations of type I collagen and validate our 3D cell migration predictions with light-sheet microscopy.

Results:

Our findings indicate that CAR-T cell migration is more sensitive to collagen concentration increases than T cells, resulting in a more pronounced reduction in their invasiveness. Moreover, our computational model reveals significant differences in 3D movement patterns between T and CAR-T cells. T cells exhibit migratory behavior in 3D whereas that CAR-T cells predominantly move within the XY plane, with limited movement in the Z direction. However, upon the introduction of a CXCL12 chemical gradient, CAR-T cells present migration patterns that closely resemble those of T cells.

Conclusions:

This framework demonstrates that 2D projections of 3D trajectories may not accurately represent real migration patterns. Moreover, it offers a tool to estimate 3D migration patterns from 2D experimental data, which can be easily obtained with automatic quantification algorithms. This approach helps reduce the need for sophisticated and expensive microscopy equipment required in laboratories, as well as the computational burden involved in producing and analyzing 3D experimental data.

* Corresponding author.
E-mail address: jmgaraz@unizar.es (J.M. Garcia Aznar).
[1] Both authors share co-first authorship.

https://doi.org/10.1016/j.cmpb.2024.108331
Received 25 March 2024; Received in revised form 5 July 2024; Accepted 16 July 2024
Available online 19 July 2024

1. Introduction

Cell migration is a key biological process that plays a crucial role in many physiological processes [1] such as wound healing [2], tissue repair [3], morphogenesis [4] and the functionality of the immune system [5]. In the context of immune response, immune cells, such as T cells and macrophages, navigate through tissues to detect and eliminate pathogens or abnormal cancer cells. However, despite their innate high migration capacity, in some cases, the natural T cells of the immune system struggle to recognize cancer cells because these can evade detection or suppress the immune response [6]. Cancer cells often employ various mechanisms to evade the immune system's surveillance, inhibiting T-cell function within the tumor microenvironment. To overcome this challenge, CAR-T cell therapy emerges as an innovative treatment strategy, leveraging engineered immune cells tailored to target specific antigens found on cancer cells [7]. This method involves the modification of a patient's T cells to express chimeric antigen receptors (CARs), thereby reprogramming these cells for enhanced recognition and targeted destruction of cancer cells with exceptional specificity. Notably, CAR-T cell therapy has demonstrated promising results in blood cancers, including lymphomas, certain forms of leukemia, and, more recently, multiple myeloma [8–10].

Nevertheless, the transformation of T cells into engineered CAR-T cells may influence their migratory capabilities. These alterations may potentially compromise their natural ability to navigate the body and reach tumor sites, thus challenging their capacity to infiltrate solid tumors effectively. This issue represents a significant obstacle to the success of CAR-T cell therapy in treating solid tumors, as opposed to its demonstrated efficacy in blood cancers. Therefore, it is crucial to comprehensively understand how these modifications impact the migratory behavior and infiltration potential of CAR-T cells to optimize their therapeutic effectiveness in solid tumor contexts.

The study of cell migration has traditionally been performed using *in vitro* [11] (e.g., the Boyden chamber migration assay [12] or scratch assay [13]) and *in vivo* (e.g., intravital microscopy [14,15] and *in vivo* imaging [16,17]) methods [18,19]. However, the use of microfluidic devices emerged as a powerful tool to study cell migration, providing a high degree of control over the microenvironment, and allowing for the study of the response of cells to specific chemical and mechanical cues [20–22]. Microfluidic devices facilitate the analysis of the impact of different extracellular matrix (ECM) properties, such as matrix density and stiffness, fiber alignment, and pore size [23,24]. Another advantage of these devices is the ability to recreate three-dimensional (3D) environments, which can provide more physiologically relevant information than two-dimensional (2D) migration assays. Furthermore, by integrating imaging systems, microfluidic devices allow for real-time monitoring of cell migration, providing information on the kinematics of cell movement and allowing for a better characterization of their motile behavior. Many different cell types have been analyzed and studied in these microfluidic-based chips: tumor cells [25,26], cancer-associated fibroblasts [27], dermal human fibroblasts [28], osteoblasts [29], leukocyte [30] among others. However, the use of microfluidic devices to study 3D immune cell migration poses a significant challenge due to their high migration capacity. While these devices can recreate 3D environments, quantification of 3D cell trajectories requires time-lapse studies integrating 2D imaging and Z-stack acquisition from the assays. Given the highly dynamic nature of 3D immune cell migration [31], it is essential to quantify a substantial number of events within a brief timeframe, which poses a risk of phototoxicity when using standard confocal microscopes. Light sheet microscopy offers a good alternative by providing low phototoxicity, high temporal resolution, and live sample imaging [31]. The primary challenge resides in managing the extensive data produced, which is complex, computationally heavy, and requires sophisticated tools for automated analysis. Apart from the technical hurdles, these microscopes represent a significant investment and are not commonly found in standard laboratory settings.

In this study, we propose a novel methodology based on agent-based models to estimate 3D cell trajectories within microfluidic devices, relying only on 2D imaging data that can be acquired even from the most basic bright-field microscope. Agent-based models offer discrete computational representations for simulating cellular behavior at a cell level, and they have been extensively employed in different areas of cell migration. For instance, [32] simulated individual and collective cell migration in glioblastoma considering the influence of the oxygen field, Gonçalves and Garcia-Aznar studied the role of collagen density in regulating cell migration and spheroid formation, Bretti and De Gaetano investigated the influence of tumor cell-produced chemical signals on immune cell dynamics within microfluidic chips, and Peng et al. explored the dynamics of cell migration within flexible channels and how mechanical interactions with the microenvironment and neighboring cells influence this process. While these approaches have focused on simulating cell migration within microfluidic devices, these works often struggle to extrapolate 3D behavior and lack a comprehensive understanding of cell migration in 3D environments.

Our lattice-free center-based agent-based model aims to predict 3D cellular behavior from 2D imaging data. To achieve this, we consider that cell locomotion direction is not entirely arbitrary but exhibits a directional bias influenced by the cell's previous orientation. To determine this directional memory, we propose an inverse sampling method to track its evolution from the previous direction. By deriving cumulative distribution functions through this sampling method, we gain insights into how past directions influence future ones. Consequently, this approach facilitates the simulation of a wide spectrum of migration behaviors, spanning from entirely persistent movement in a single direction when the cumulative distribution function approximates a Heaviside function, to non-persistent random movement devoid of directional persistence when the function takes on a linear shape. Finally, we apply the proposed methodology to simulate migration assays involving CAR-T cells and natural T cells (serving as the control group) within distinct collagen concentration matrices within microfluidic-based devices. The resulting 3D migration patterns are then compared and validated with experimental 3D measurements obtained through a lattice light-sheet microscope. Our results underscore the variances between 2D projections and genuine 3D motion, revealing that CAR-T cells display diminished motility in 3D relative to natural T cells.

2. Methods

2.1. Computational framework for predicting 3D migration patterns

We present a computational framework for predicting 3D migration of cells in microfluidic devices using 2D *in vitro* data (Fig. 1). In this experimental setup, cells are seeded individually into microfluidic devices, and their movements are live-tracked within a single plane by capturing images at regular time intervals of Δt. These tracked cells are adequately spaced apart to prevent interactions between them, enabling the study of their individual migration dynamics. Then, we acquire individual cell trajectories and instantaneous velocities for each cell. Subsequently, we calculate the mean velocity of each cell and determine the overall mean of these individual mean velocities across the entire population $\bar{v}_c$.

The computational model consists of a 3D center-based lattice-free agent-based model. Thus, the balance of forces acting on a single-moving cell is:

$$m_c \frac{d\boldsymbol{v}_c(t)}{dt} = \boldsymbol{F}_{loc}(t) + \boldsymbol{F}_{drag}(t) \approx 0. \tag{1}$$

Here, m_c is the mass of the cell, $\boldsymbol{v}_c(t)$ is its velocity, $\boldsymbol{F}_{loc}(t)$ represents the cell's locomotive force for migration, and $\boldsymbol{F}_{drag}(t)$ represents the friction force of the cell with the matrix. In this expression, the inertia term is typically neglected due to the small mass and velocity of the cell. The friction force is calculated using Stokes' law, which is

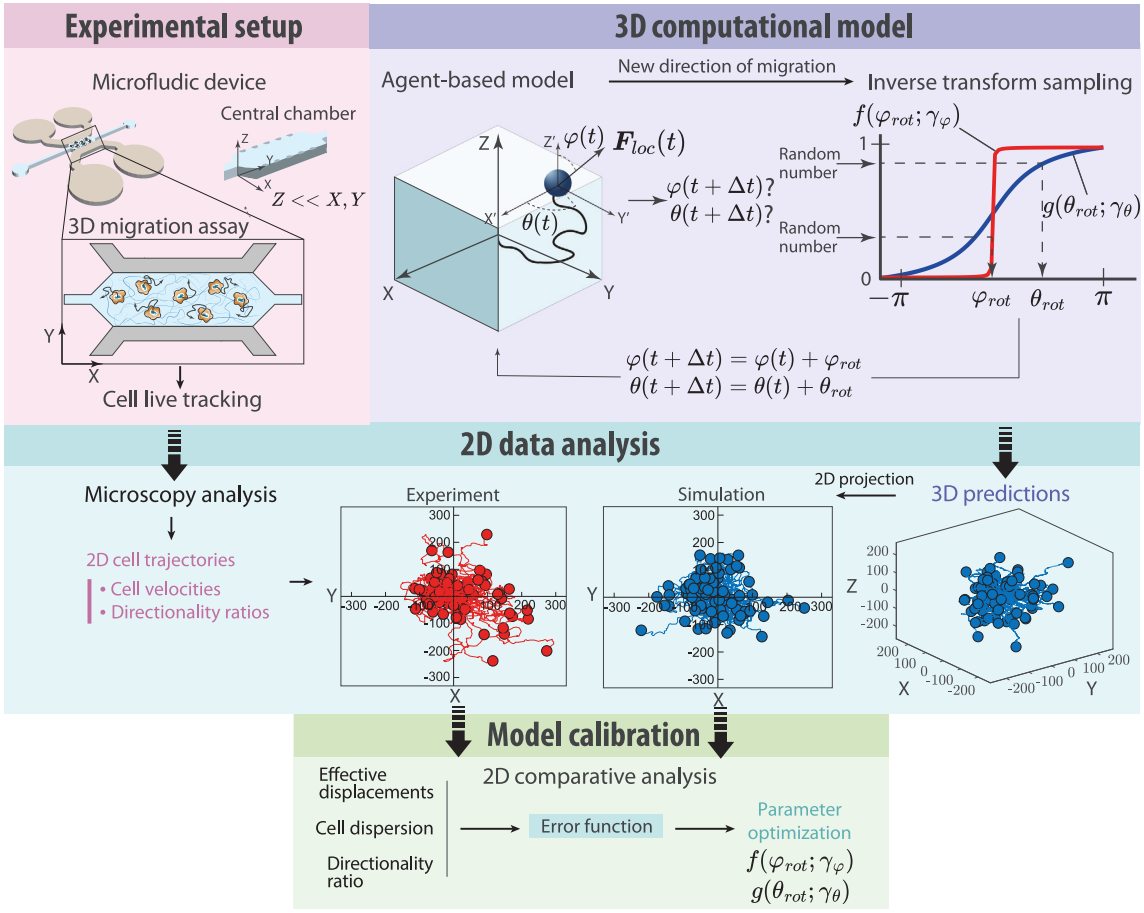

Fig. 1. Overview of the 3D migration framework. In the experimental setup, N individual cells are initially seeded onto a microfluidic device and tracked over t_{sim} duration, capturing 2D images at intervals of Δt. Concurrently, N 3D simulations of a single moving cell are performed using the agent-based model. The direction of the locomotive force is determined by angles $\theta(t)$ and $\varphi(t)$. To simulate the temporal direction of the locomotive force $\boldsymbol{F}_{loc}(t)$, we implement an inverse transform sampling method. This technique calculates rotational angles θ_{rot} and φ_{rot} using cumulative distribution functions $f(\varphi_{rot};\gamma_\varphi)$ and $g(\theta_{rot};\gamma_\theta)$ respectively. After completing the simulations, we evaluate the accuracy of the simulations by projecting the 3D predictions into 2D and comparing them with the experiments. Thus, we calculate the error between the simulation and experiment of the mean effective displacement, cell dispersion, and the directionality ratio. Subsequently, we update the functions $f(\varphi_{rot};\gamma_\varphi)$ and $g(\theta_{rot};\gamma_\theta)$ until the error between the simulation and experiment is minimized.

appropriate for modeling the movement of spherical particles in a viscous fluid under laminar flow conditions:

$$\boldsymbol{F}_{drag}(t) = 6\pi R_c \eta \boldsymbol{v}_c(t), \tag{2}$$

with $R_c = 10$ μm the radius of the cell and η the dynamic viscosity of the collagen hydrogel obtained from Valero et al.. Considering that the magnitude of the locomotive force is constant but variable in direction:

$$\boldsymbol{F}_{loc}(t) = F_{loc}\boldsymbol{e}(t) = 6\pi R_c \eta \bar{v}_c \boldsymbol{e}(t), \tag{3}$$

where $\bar{v}_c$ is the overall mean velocity of the experiment and $\boldsymbol{e}(t) = (e_\theta(t), e_\varphi(t))$ is the unit orientation vector in spherical coordinates $(r, \theta(t), \varphi(t))$. We simulate the temporal changes in the migration direction $(\theta(t), \varphi(t))$ through a rotational transformation:

$$\begin{aligned}\theta(t+\Delta t) &= \theta(t) + \theta_{rot},\\ \varphi(t+\Delta t) &= \varphi(t) + \varphi_{rot}.\end{aligned} \tag{4}$$

Here, θ_{rot} and φ_{rot} are the rotations of the azimuthal and polar angles respectively. To determine these rotations, we consider that the migration direction exhibits a directional bias influenced by its prior orientation and propose an inverse transform sampling method. This method involves generating pseudo-random numbers from a uniform distribution and applying the inverse cumulative distribution function (CDF) associated with the desired probability distribution. Specifically, we utilize the CDF of the Cauchy function:

$$C(a; a_0, \gamma) = \frac{1}{\pi}\arctan\left(\frac{a-a_0}{\gamma}\right) + \frac{1}{2}, \tag{5}$$

with $a_0 = 0$ to be centered at $x = 0$, and γ a parameter that controls the function's shape. To account for potential variations in rotations for $\theta(t)$ and $\varphi(t)$, we utilize two analogous functions, denoted as $f(\varphi_{rot};\gamma_\varphi)$ and $g(\theta_{rot};\gamma_\theta)$, derived from the same form as the CDF in Eq. (5) within the inverse transform sampling method. Thus, we use this technique to generate values for θ_{rot} and φ_{rot} within the interval $(-\pi, \pi)$, allowing for the calculation of the new directional angles $\theta(t+\Delta t)$ and $\varphi(t+\Delta t)$ through Eq. (4).

After simulating N single migrating cells in 3D, we project the trajectories in 2D for a direct comparison with the experimental data. For model calibration, we employ prediction metrics involving the cell trajectories $(\boldsymbol{x}_c(t))$ and directionality ratio $(d_r(t))$ (see Supplementary 1 for directionality ratio details). In particular, we determine the mean effective displacement of cells along the X $\left(s_x = (\bar{x}_c(t = t_{sim}))\right)$ and Y $\left(s_y = (\bar{y}_c(t = t_{sim}))\right)$ axes and integrate it into the metric $s_{xy} = \sqrt{s_x^2 + s_y^2}$. Similarly, we calculate the standard deviation of cells' final positions along the X (σ_x) and Y (σ_y) directions to estimate cell invasion and incorporate this information into a comprehensive metric, $\sigma_{xy} = \sqrt{\sigma_x^2 + \sigma_y^2}$, to capture cell dispersion over the XY plane. We also calculate the area under the curve of the mean XY directionality ratio $(\bar{d}_r(t))$ of cells $\left(D_r = \int_{t=0}^{t=t_{sim}} \bar{d}_r(t)\, dt\right)$ to evaluate the cell trajectories'

straightness. Then, we compute the error between the simulation and experimental metrics through Gaussian-like functions of the form:

$$h(a,b) = \exp\left(-\frac{(a-b)^2}{2\left(b^2\right)}\right). \quad (6)$$

Thus, the error is calculated as:

$$\mathcal{E} = 1 - \left(\frac{1}{3}h(s_{xy}^{sim}, s_{xy}^{exp}) + \frac{1}{3}h(\sigma_{xy}^{sim}, \sigma_{xy}^{exp}) + \frac{1}{3}h(D_r^{sim}, D_r^{exp})\right). \quad (7)$$

Finally, we minimize the error ($\mathcal{E}$) using a direct search optimization method, iteratively updating γ_φ and γ_θ while minimizing the error ($\mathcal{E}$) to obtain the functional shapes of $f(\varphi_{rot};\gamma_\varphi)$ and $g(\theta_{rot};\gamma_\theta)$ that accurately reproduce cell migration within the microfluidic devices.

2.2. Fabrication of microfluidic devices

Microfluidic chips were fabricated in PDMS (polydimethylsiloxane-Dow Corning GMbH Sylgard 184) at a 10:1 ratio of base to curing agent, following the methodology described by Shin et al.. PDMS microdevices were plasma-bonded to 35 mm glass-bottom Petri dishes (IBIDI) and treated with poly-D-lysine (PDL) solution (Sigma-Aldrich) at 1 mg/mL to enhance the surface-matrix attachment. The geometry of the microfluidic devices consisted of a central chamber in which we introduced the hydrogel with the cells and two adjacent media channels that allowed the introduction of cell culture medium and the generation of chemical gradients through the addition of a growth factor CXCL12 in one of the channels [37]. The study previously published by Moreno-Arotzena et al. presents further details about the geometry of these microfluidic devices.

2.3. Cell culture and transduction of primary human T cells

PBMCs were obtained by Ficoll-Paque gradient centrifugation from blood obtained from Healthy Donors (CEICA, C.I. PI 11/006). They were activated with anti-CD3 (OKT3 clone) and anti-CD28 antibodies (BD Pharmingen) in complete medium; 44% RPMI1640 (PAN Biotech) + 44% Click's médium (Sigma) + 10% FBS (Sigma) + 1% Glutamax (Gibco) + 1% Pen/Strep, (Sigma). The next day, the medium was supplemented with IL-7 and IL-15 (Miltenyi Biotec) at a final concentration of 10 ng/mL. The transduction was performed on the third day with lentiviral vector supernatants as described by Davies et al. and Vectofusin-1 (Miltenyi Biotec) according to the manufacturer's recommendations. The activated PBMCs followed the same steps but without lentiviral vector supernatants. After centrifugation, the medium was replaced with fresh medium with IL-4 at 30 ng/mL (Miltenyi Biotec). The medium was replaced every two or three days with fresh medium with IL-4.

2.4. Hydrogel preparation and 3D cell culture

The hydrogels were prepared using collagen gel solution type I (BD Bioscience) to a final concentration of 4 and 6 mg/mL, following the methodology proposed by [20]. The dilution was brought to pH 7.4 with 0.5M NaOH. T cells and CAR T4 were suspended in a culture medium and mixed with the collagen hydrogel to a final dilution of 1.5×10^5 cells/ml to follow individual migration in 3D. For light-sheet microscopy (LLSM) 6 mg/mL collagen gels were used. The final dilution of cells was 1×10^6 cells/mL which were stained with 1 mM Vibrant DiO (Molecular Probes) at 37 °C for 30 min. Then, the cells were spun down, rinsed, and resuspended in a fresh medium. The dilution of cells was then pipetted into the central gel chamber and the hydrogel was confined by surface tension. Once in place, the collagen gel solution was polymerized in a humidity chamber at 37 °C and 5% CO_2 for 20 min. After that, the matrix was hydrated with RPMI 1640 (Lonza) supplemented with 10% FBS, 1% penicillin/streptomycin (Sigma-Aldrich), 1% GlutaMAX (Thermo Fischer), and 30 ng/mL IL4 (Miltenyi Biotec).

2.5. Image acquisition and quantification of T cells and CAR-T4 migration

Cell migration was recorded using time-lapse live microscopy (Nikon D-Eclipse Ti Microscope and Zeiss Axio Observer 7) with a 10X objective for migration, acquiring phase contrast images every 30 s for 1 h. The focal plane was chosen to be in the middle along the z-axis of the device ensuring that the tracked cells were embedded within the 3D network. Cell trajectories were obtained using IMAGEJ and further analyzed using MATLAB scripts.

3D live T cell and CAR-T4 migration with light-sheet microscopy (LLSM) on a ZEISS Lattice Light Sheet 7 microscope (ZEISS, Oberkochen, Germany) was followed during 1.5 h exciting the cells at 488 nm. For all experiments, the datasets acquired were deskewed using the ZEISS Zen (blue edition 3.7) software by a linear interpolation and a Cover-glass transformation. Deconvolution was performed using a constrained iterative algorithm. The resulting images had a voxel size of $0.14 \times 0.14 \times 0.14$ μm^3 and image stacks had a mean temporal resolution of 169.8 ± 26.34 s per frame. For further processing, sample image stacks were resized with the resampling method of ZEISS's software to 1/8 of their original size, reaching a voxel size of $1.16 \times 1.16 \times 1.16$ μm^3, reducing significantly data size for easier management. During the experiment, the incubation conditions were controlled and held at 37 °C, 5% CO_2, and 95% of humidity. The experiments with 4 mg/mL collagen matrices were performed with two independent experiments, with four technical replicas for T cells and for CAR-T4, and the experiments with 6 mg/mL with two independent experiments and four technical replicas with T cells and with four independent experiments with six technical replicas with CAR-T4. For the assays with CXCL12 in 6 mg/mL collagen, two experiments were performed with three technical replicas. 3D experiment with light-sheet microscopy was performed once with two technical replicas with T cells and three with CAR-T4.

3. Results

3.1. CAR-T cell migration is more sensitive to collagen concentration than T cells

To demonstrate the potential of the computational framework in accurately replicating cell movement patterns, we first conduct cell migration assays of T and CAR-T4 cells (hereinafter referred to as CAR-T) within microfluidic devices embedded in collagen-based hydrogels. These cells are individually seeded in two distinct concentrations of type I collagen (4 and 6 mg/mL), replicating the extracellular environment. The microfluidic device consists of a central chamber with an embedded collagen matrix containing cells and two lateral channels serving as reservoirs for growth media. In some cases, the chemoattractant CXCL12 is introduced into one of the channels to establish a chemotactic gradient within the microfluidic devices with 6 mg/mL of collagen. Live-cell imaging techniques in 2D are employed, capturing images at 30-second intervals for 1 h to track cell movement. Subsequently, we characterize the migration patterns using the proposed calibration metrics (Table 1, experiments column).

Then, we apply the proposed methodology to gain insights into the 3D behavior of cells, replicating the 2D microfluidic device migration assays. The calibration metrics derived from the experimental data are matched with the simulations (Table 1, simulation column), and the shape of the functions $f(\varphi_{rot};\gamma_\varphi)$ and $g(\theta_{rot};\gamma_\theta)$, which determine the directionality of cell migration, is obtained (Fig. 2**B**). Note how the optimized functions exhibit very subtle differences, yet these nuances have a significant impact on the outcomes.

The 2D projections of our 3D simulations replicated the cell trajectories of T and CAR-T cells in various collagen matrices (Fig. 2**C**). Our observations reveal that at a collagen concentration of 4 mg/mL, T cells and CAR-T cells exhibit a similar mean displacement in the XY plane. However, T cells show more directional movement (8.54%

Table 1
Experiments and simulation data. N is the number of cells, $\bar{v}_c$ is the overall mean velocity of the cells, s_{xy} is the module of the mean effective displacement of cells along the X and Y axes, the σ_{xy} indicates the module of the standard deviation of cells' final positions along the X and Y directions, D_r is the area under the curve of the mean XY directionality ratio of cells, and $\mathcal{E}$ is the error between the experiments and the simulation calculated through Gaussians-like functions from (7).

Cell type	Medium	N	Experiments				Simulations			$\mathcal{E}$ (%)
			$\bar{v}_c$ (μm/min)	s_{xy} (μm)	σ_{xy} (μm)	D_r	s_{xy} (μm)	σ_{xy} (μm)	D_r	
T	4 mg/mL	75	6.80	81.12	110.64	22.32	84.00	108.41	23.46	0.33
	6 mg/mL	44	5.26	52.40	81.64	19.20	55.89	73.09	19.10	1.17
CAR-T	4 mg/mL	31	6.53	80.17	122.04	20.41	86.24	109.40	21.98	1.70
	6 mg/mL	49	3.94	41.57	70.15	18.11	45.76	59.66	20.35	3.60
	6 mg/mL + CXCL12	27	4.30	51.22	78.42	26.67	51.70	71.36	26.51	0.63

greater) and less dispersion (9.3% lower) than CAR-T cells. At a collagen concentration of 6 mg/mL, T cells reduce their mean displacement by 35.5%, while CAR-T cells exhibit a more substantial reduction of 48.2%. Similarly, dispersion decreases more in the case of CAR-T (42.6%) compared to T cells (26.2%), and directionality is also lower in CAR-T compared to T cells. Furthermore, although the velocities are similar at 4 mg/mL, at 6 mg/mL the overall mean velocity of T cells decreases by 22.7%, while for CAR-T cells, the decrease is 39.6%. This highlights a markedly higher sensitivity of CAR-T cells to collagen density alterations, resulting in a 20.6% smaller mean displacement, 14.1% smaller dispersion, and 25.10% smaller velocity compared to T cells under similar 6 mg/mL conditions. Nonetheless, the introduction of the chemo-attractant CXCL12 to the 6 mg/mL matrix leads to a 23.25% increase in XY plane displacement, an 11.7% increase in dispersion, and 9.14% increase in velocity, narrowing the gap between CAR-T and T cells' mean displacement and dispersion to 2.2% and 3.9%, respectively, and making migration more persistent (47.3% greater than the condition without CXCL12).

To further validate the accuracy of our replications of 2D cell movement, we analyze the effective displacements along the X and Y axes, revealing no statistically significant differences between simulation predictions and experimental displacements derived from *in vitro* data (Fig. 2**D**). Additionally, we assess the directionality ratio for T and CAR-T cells in different matrices, confirming its ability to capture the temporal evolution of the experimental data (Fig. 2**E**).

3.2. CAR-T cells tend to move in 2D, in contrast to the patterns observed in T cells

In this section, we present model predictions of 3D trajectories for T and CAR-T cells in different matrices (Fig. 3**A**), providing an isometric view of the 2D projected trajectories in Fig. 2**C**. Despite the apparent similarity in 2D invasion patterns, as shown before, significant disparities are observed in the 3D movement patterns between T and CAR-T cells. While T cells exhibit multi-directional migration, CAR-T cells show a limited movement along the Z-axis, suggesting predominantly 2D movement at both 4 and 6 mg/mL. To quantify these results, we compare the effective displacement along the X and Y-axis with the effective displacements along the Z-axis (Fig. 3**B**). At both 4 and 6 mg/mL matrices, T cells demonstrate a more balanced movement across the X, Y, and Z axes, with a ratio between the median displacement in the Z direction and the XY directions of 1.01 and 0.95, respectively. In contrast, CAR-T cells at the same concentration matrices exhibit predominantly favored movement in the XY plane, with a ratio between the median displacement in the Z direction and the X and Y directions of about 0.60 for both 4 and 6 mg/mL. However, the introduction of CXCL12 to the 6 mg/mL matrix significantly boosts the Z-axis movement for CAR-T cells, resulting in the most remarkable 3D movement observed in this scenario, with a median displacement in the Z direction 2.16 times higher than in the X and Y. We find no statistically significant differences between the effective displacements on the XY plane and Z in T cells but identify significant differences for CAR-T cells, suggesting the tendency of CAR-T cells to move two-dimensionally in the 4 and 6 mg/mL matrices not enriched with CXCL12.

To confirm these predictions of the 3D movement patterns, we conduct new 3D *in vivo* migration experiments, tracking T and CAR-T cells in real-time for 1.5 h within a 6 mg/mL hydrogel. This 3D experiment, utilizing light-sheet microscopy, provides a more detailed understanding of cell migration within a 3D environment, allowing for the study of their spatial behavior. Subsequently, we calculate the ratio between the movement in the Z direction and the planar XY movement for each displacement (Fig. 3**C**). Our observations reveal that T cells exhibited 3D movement, with a ratio between Z and XY movements of 0.93. In contrast, CAR-T cells predominantly move in the XY plane with a ratio between Z and XY movements of 0.57. We find no statistically significant differences between simulations and experiments but we do find a significant difference in movement patterns between T cells and CAR-T cells, confirming the model predictions of a more predominant 2D movement pattern of CAR-T cells compared to T cells.

4. Discussion

In this work, we developed a computational framework to estimate 3D migration patterns of cells within microfluidic environments using an agent-based model, relying exclusively on 2D *in vitro* measurements. To assess the predictive capabilities of our model, we simulated *in vitro* migration experiments of T and CAR-T cells in hydrogels with different concentrations of type I collagen in microfluidic devices. We showed that the 2D projections of our 3D predictions successfully reproduced the 2D migration patterns of both T and CAR-T cells in the different density matrices, with no statistically significant differences between the experiments and simulations (Fig. 2). Moreover, we observed that although CAR-T and T cells behaved similarly at 4 mg/mL, CAR-T cells showed higher susceptibility to the increment in collagen concentration compared to T cells, resulting in a more pronounced reduction in their invasiveness.

Furthermore, our computational model revealed notable differences in the 3D movement patterns between T and CAR-T cells. T cells displayed migratory behavior in three dimensions within the two collagen concentration matrices, aligning with the characteristic high motility observed in immune cells that enables their access to intricate regions within the body. In contrast, our simulations unveiled a distinctive pattern in CAR-T cells. They appeared to predominantly move within the XY plane and exhibited limited movement in the Z direction, indicative of primarily 2D migration. To quantify the differences between movements in each direction, we calculated the displacement ratio between the Z direction and the X and Y directions. T cells presented a ratio around 1 in both density matrices, indicating a balanced three-dimensional movement, while CAR-T cells presented a ratio around 0.6 in both matrices, emphasizing their predisposition to move more over the XY plane compared to the Z direction. We found no statistically significant difference between the Z and XY displacements in the case

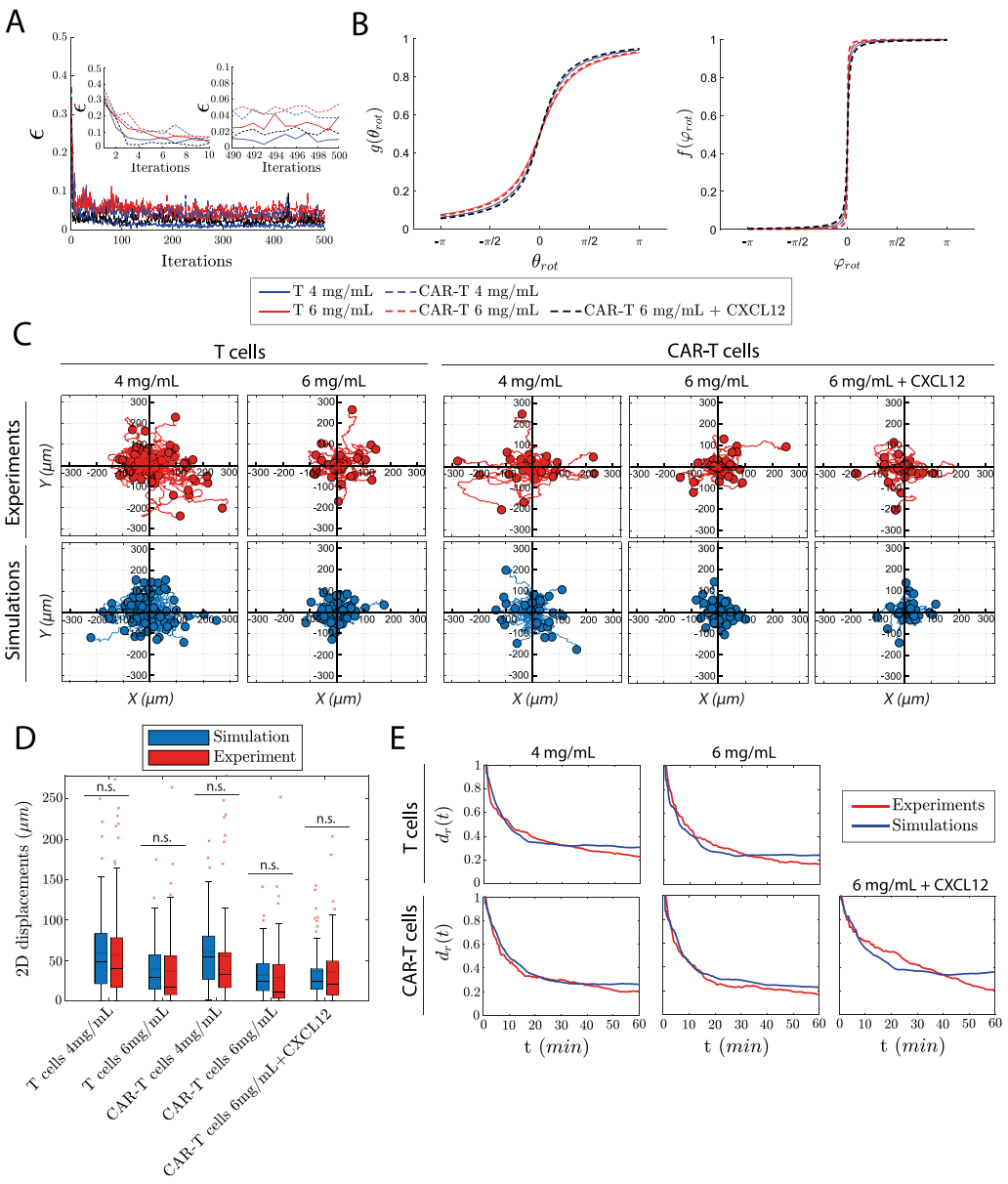

Fig. 2. Comparative analysis of 2D cell migration patterns between experiments and simulations. **A.** Calibration errors for each iteration of minimization, with two details at the first and last 10 iterations. **B.** Obtained directional migration functions $g(\theta_{rot};\gamma_\theta)$ and $f(\varphi_{rot};\gamma_\varphi)$ from the inverse transform sampling method that minimize calibration error. **C.** Experimental and simulated 2D cell trajectories of T and CAR-T cells in different collagen density matrices. **D.** Analysis of effective displacements along X and Y axes between experiments and simulations. ANOVA followed by post hoc Tukey–Kramer tests are performed to determine statistical significance. $***$ $P < 0.001$; $**$ $P < 0.01$; $*$ $P < 0.05$. We find no statistically significant differences between experiment and simulation results in any of the conditions. **E.** Comparison of simulated and experimental directionality curves.

of T cells, but we did find notable differences in the Z movement compared to the XY movement in the case of CAR-T cells.

To validate these results of our new approach, we conducted 3D cell migration experiments at 6 mg/mL using light-sheet microscopy, allowing us to quantify cell migration patterns in 3D. Similarly, we calculated, for each displacement, the ratio between the Z movement and the mean X and Y movements, showing that in 3D experiments, T cells exhibited three-dimensional movement (Z movement versus mean XY movement of 0.93), whereas CAR-T cells exhibited limited movement along the Z axis (Z movement versus mean XY movement of 0.57). We compared these experimental observations with our simulations and found no statistically significant differences between them. However, we did observe differences between T and CAR-T cells, confirming the model's predictions of 3D migration patterns derived from 2D data. Additionally, our investigation revealed that the presence of the chemical factor CXCL12 not only stimulated CAR-T cells to migrate within the XY plane but also induced a shift in behavior, promoting 3D movement similar to T cells. Therefore, enhancing the migrative capacity of CAR-T cells might be a promising strategy to improve the efficacy of therapies in solid tumors [39].

The planar migration pattern observed in CAR-T cells may be attributed to two main factors. Firstly, the exposure of T-cells to chimeric antigen receptors during their conversion into CAR-T cells could influence their migration capabilities, potentially reducing their ability to navigate through intricate and confined spaces. CAR-T cells can be designed for different chimeric antigen receptors, depending on the targeting tumor-associated antigen. In this study, EGFR-targeted CAR-T cells were generated, which may impact cell motility differently compared to other conversions. Secondly, the geometrical characteristics of microfluidic devices must be considered. The fiber alignment in the XY plane that is produced in microfluidic devices when pipetting the hydrogel through the narrow lateral microchannels into the central chamber, combined with the geometrical dimensions of the central chamber (where the Z dimension is much smaller than the X and Y

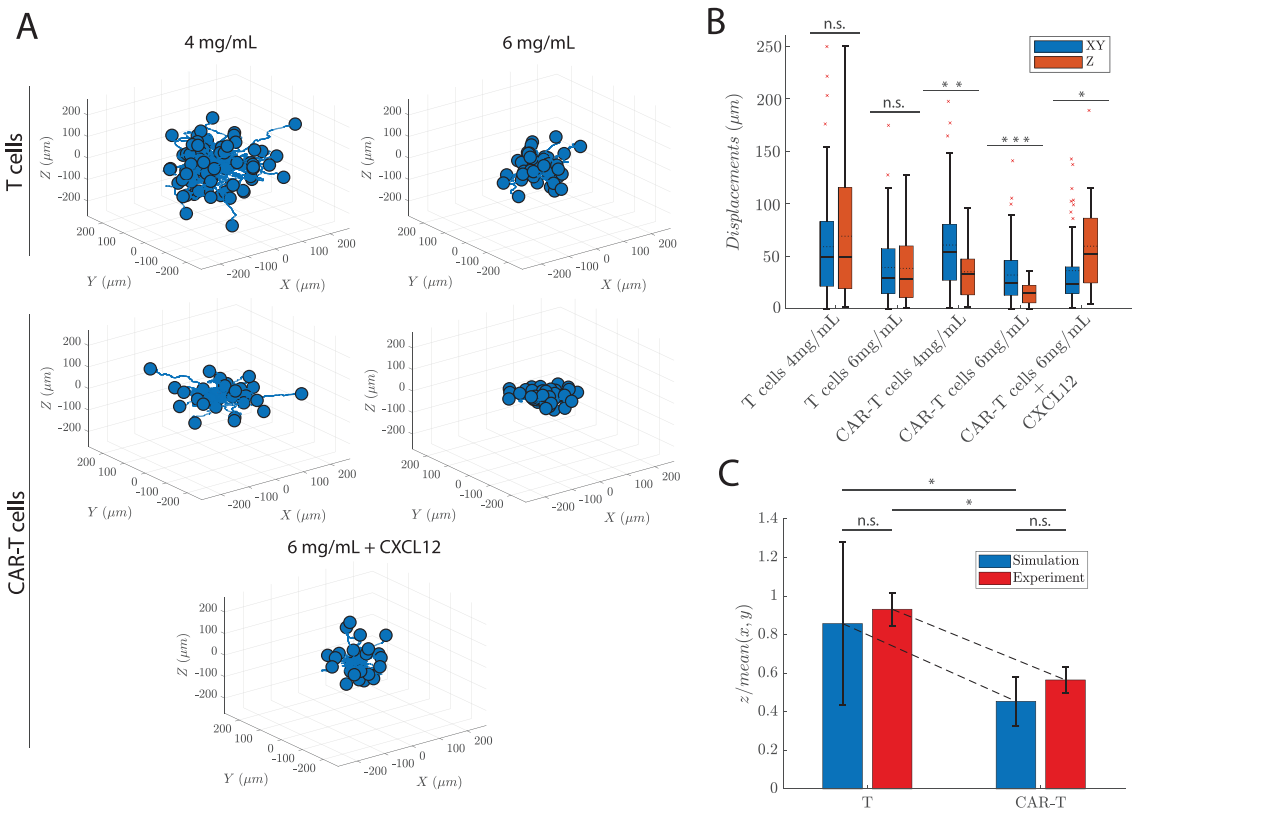

Fig. 3. Analysis of 3D cell migration patterns. **A.** Isometric view of the 3D predictions of cell trajectories for T and CAR-T cells corresponding to the 2D simulated trajectories in Fig. 2**C. B.** Analysis of effective displacements along the X and Y axes versus the Z axis in the simulations for T and CAR-T cells in different matrices. ANOVA followed by post hoc Tukey–Kramer tests are performed to determine statistical significance. *** $P < 0.001$; ** $P < 0.01$; * $P < 0.05$. We find statistically significant differences between the CAR-T movement pattern in the X and Y directions and the Z direction in all conditions, in contrast with the T cells which present similar patterns. **C.** Comparison of the ratio of effective displacement in the Z direction and the mean effective displacement in the X and Y directions between simulations and the 3D *in vivo* experiment in the 6 mg/mL matrix. We find no statistically significant differences between simulations and experiments, but we do find statistically significant differences between T and CAR-T cells.

dimensions), generates a less confined environment in the X and Y directions [40–42]. We suggest that this alignment in the XY plane might be affecting the migration patterns of CAR-T cells, which may find difficulties in moving against the direction of the fibers. This influence could lead to a reduction in migration, potentially transitioning from 3D movement to a mode resembling 2D migration. The combination of these factors may account for the observed behavior, further limiting the cells' ability to migrate in the Z direction within this complex environment.

Nevertheless, we have to keep in mind that our novel predictive approach is based on several simplifications. Initially, we assumed cells exert constant magnitude locomotive force, with temporal changes attributed solely to changes in migration direction. Cells may generate locomotive forces varying in both magnitude and direction. However, to calculate this force magnitude, we used the temporal mean velocity of the entire cell population. This mean velocity represents the temporal velocity variations across the cell population. Therefore, considering a mean locomotive force effectively encompasses the temporal variations in force magnitude across the population of cells, offering a comprehensive measure of these temporal fluctuations and modeling it with a mean representative value. However, temporal variations in the locomotive force magnitude can be easily incorporated, for instance, making it variable within a certain range. Temporal variations in the magnitude of the locomotive force can be easily incorporated by allowing it to vary within a certain range, based on probability distributions derived from velocity measurements. Additionally, we utilized the displacements, dispersion, and directionality ratio as predictive metrics. While projecting trajectories in 2D can yield the same trajectories across multiple positions, the combination of these predictive metrics, in conjunction with cell velocity, constrains the feasible cell positions that result in XY projections. Thus, to infer 3D movement, it is necessary to have sufficient 2D data, including a sufficient number of cells and XY movement, to ensure that the proposed metrics represent the collective behavior of cell migration patterns. Nonetheless, further refinements could be incorporated during the calibration phase, as the model can be easily tailored to the user's needs. For example, additional criteria could be added to better capture the directionality ratio over time, taking into account not only the area under the curve but the value of the ratio at different time steps. Similarly, our approach possesses the flexibility to incorporate additional metrics based on the specific in-vitro data collected, demonstrating its adaptability for various types of migration assays.

Therefore, the methodology here proposed can be used by researchers to estimate 3D migration patterns from 2D experimental data which can be easily obtained with automatic quantification algorithms [43,44]. This approach helps reduce the need for sophisticated and expensive microscopies required in laboratories, as well as the computational burden involved in producing and analyzing 3D experimental data.

CRediT authorship contribution statement

Daniel Camacho-Gomez: Writing – original draft, Visualization, Validation, Software, Methodology, Investigation, Formal analysis, Conceptualization. **Nieves Movilla:** Writing – review & editing, Methodology. **Carlos Borau:** Writing – review & editing, Methodology. **Alejandro Martin:** Methodology. **Carmen Oñate Salafranca:** Methodology. **Julian Pardo:** Resources, Methodology. **Maria Jose Gomez-Benito:** Writing – review & editing, Supervision. **Jose Manuel Garcia-Aznar:** Writing – review & editing, Supervision, Resources, Project administration, Funding acquisition, Conceptualization.

Declaration of competing interest

None Declared.

Acknowledgments

This research was funded by the European Research Council (ICoMICS Adv grant agreement: 101018587, J.M.G.A., M.J.G.B., N.M.), and Next Generation EU (ProCanAid Grant No. PLEC2021-007709, D.C.G., J.M.G.A., M.J.G.B.). J.P.'s lab is funded by AEI (Agencia Estatal de Investigación) PID2020-113963RBI00, Aragon Government (B29-20R), Health National Institute Carlos III (CIBERINFEC, CB21/13/00087 and Programa Fortalece FORT23/00028), Asociación Española Contra el Cancer (AECC), ASPANOA y Carrera de la mujer de Monzon. M.C.O is supported by a PTA contract from AEI.

Code availability

Original codes are available at https://github.com/daniel-camacho-gomez/2D_Data-to-3D_Migration

Appendix A. Supplementary data

Supplementary material related to this article can be found online at https://doi.org/10.1016/j.cmpb.2024.108331.

References

[1] Xavier Trepat, Zaozao Chen, Ken Jacobson, Cell migration, Compr. Physiol. 2 (4) (2012) 2369, http://dx.doi.org/10.1002/cphy.c110012.
[2] Li Li, Yong He, Min Zhao, Jianxin Jiang, Collective cell migration: Implications for wound healing and cancer invasion, Burns Trauma 1 (1) (2013) 2321–3868, http://dx.doi.org/10.4103/2321-3868.113331.
[3] Xiaorong Fu, Ge Liu, Alexander Halim, Yang Ju, Qing Luo, Guanbin Song, Mesenchymal stem cell migration and tissue repair, Cells 8 (8) (2019) 784, http://dx.doi.org/10.3390/cells8080784.
[4] Maik C Bischoff, Sebastian Lieb, Renate Renkawitz-Pohl, Sven Bogdan, Filopodia-based contact stimulation of cell migration drives tissue morphogenesis, Nat. Commun. 12 (1) (2021) 791, http://dx.doi.org/10.1038/s41467-020-20362-2.
[5] Paulus Mrass, Wolfgang Weninger, Immune cell migration as a means to control immune privilege: lessons from the CNS and tumors, Immunol. Rev. 213 (1) (2006) 195–212, http://dx.doi.org/10.1111/j.1600-065X.2006.00433.x.
[6] Theresa L. Whiteside, Immune suppression in cancer: effects on immune cells, mechanisms and future therapeutic intervention, in: Seminars in Cancer Biology, Vol. 16,1, Elsevier, 2006, pp. 3–15, http://dx.doi.org/10.1016/j.semcancer.2005.07.008.
[7] Sophia Stock, Michael Schmitt, Leopold Sellner, Optimizing manufacturing protocols of chimeric antigen receptor T cells for improved anticancer immunotherapy, Int. J. Mol. Sci. 20 (24) (2019) 6223, http://dx.doi.org/10.3390/ijms20246223.
[8] Hassan Dana, Ghanbar Mahmoodi Chalbatani, Seyed Amir Jalali, Hamid Reza Mirzaei, Stephan A Grupp, Eloah Rabello Suarez, Catarina Rapôso, Thomas J Webster, CAR-T cells: Early successes in blood cancer and challenges in solid tumors, Acta Pharmaceut. Sinica B 11 (5) (2021) 1129–1147, http://dx.doi.org/10.1016/j.apsb.2020.10.020.
[9] Nico Gagelmann, Kristoffer Riecken, Christine Wolschke, Carolina Berger, Francis A Ayuk, Boris Fehse, Nicolaus Kröger, Development of CAR-T cell therapies for multiple myeloma, Leukemia 34 (9) (2020) 2317–2332, http://dx.doi.org/10.1038/s41375-020-0930-x.
[10] Fumou Sun, Yan Cheng, Visanu Wanchai, Wancheng Guo, David Mery, Hongwei Xu, Dongzheng Gai, Eric Siegel, Clyde Bailey, Cody Ashby, et al., Bispecific BCMA/CD24 CAR-T cells control multiple myeloma growth, Nat. Commun. 15 (1) (2024) 615, http://dx.doi.org/10.1038/s41467-024-44873-4.
[11] Nina Kramer, Angelika Walzl, Christine Unger, Margit Rosner, Georg Krupitza, Markus Hengstschläger, Helmut Dolznig, In vitro cell migration and invasion assays, Mutat. Res./Rev. Mutat. Res. 752 (1) (2013) 10–24, http://dx.doi.org/10.1016/j.mrrev.2012.08.001.
[12] Hong-Chen Chen, Boyden chamber assay, in: Cell Migration, Springer, 2005, pp. 15–22, http://dx.doi.org/10.1385/1-59259-860-9:015.
[13] Chun-Chi Liang, Ann Y. Park, Jun-Lin Guan, In vitro scratch assay: a convenient and inexpensive method for analysis of cell migration in vitro, Nat. Protoc. 2 (2) (2007) 329–333, http://dx.doi.org/10.1038/nprot.2007.30.
[14] Roberto Weigert, Monika Sramkova, Laura Parente, Panomwat Amornphimoltham, Andrius Masedunskas, Intravital microscopy: a novel tool to study cell biology in living animals, Histochem. Cell Biol. 133 (5) (2010) 481–491, http://dx.doi.org/10.1007/s00418-010-0692-z.
[15] Evelyne Beerling, Laila Ritsma, Nienke Vrisekoop, Patrick WB Derksen, Jacco van Rheenen, Intravital microscopy: new insights into metastasis of tumors, J. Cell Sci. 124 (3) (2011) 299–310, http://dx.doi.org/10.1242/jcs.072728.
[16] Elizabeth MC Hillman, Cyrus B Amoozegar, Tracy Wang, Addason FH McCaslin, Matthew B Bouchard, James Mansfield, Richard M Levenson, In vivo optical imaging and dynamic contrast methods for biomedical research, Phil. Trans. R. Soc. A 369 (1955) (2011) 4620–4643, http://dx.doi.org/10.1098/rsta.2011.0264.
[17] Hideki Yamaguchi, Jeffrey Wyckoff, John Condeelis, Cell migration in tumors, Curr. Opin. Cell Biol. 17 (5) (2005) 559–564, http://dx.doi.org/10.1016/j.ceb.2005.08.002.
[18] Frank Entschladen, Theodore L Drell IV, Kerstin Lang, Kai Masur, Daniel Palm, Philipp Bastian, Bernd Niggemann, Kurt S Zaenker, Analysis methods of human cell migration, Exp. Cell Res. 307 (2) (2005) 418–426, http://dx.doi.org/10.1016/j.yexcr.2005.03.029.
[19] Daniel Palm, Kerstin Lang, Burkhard Brandt, Kurt S Zaenker, Frank Entschladen, In vitro and in vivo imaging of cell migration: two interdepending methods to unravel metastasis formation, Sem. Cancer Biol. 15 (5) (2005) 396–404, http://dx.doi.org/10.1016/j.semcancer.2005.06.008.
[20] Yoojin Shin, Sewoon Han, Jessie S Jeon, Kyoko Yamamoto, Ioannis K Zervantonakis, Ryo Sudo, Roger D Kamm, Seok Chung, Microfluidic assay for simultaneous culture of multiple cell types on surfaces or within hydrogels, Nat. Protoc. 7 (7) (2012) 1247–1259.
[21] O Moreno-Arotzena, G Mendoza, M Cóndor, T Rüberg, JM García-Aznar, Inducing chemotactic and haptotactic cues in microfluidic devices for three-dimensional in vitro assays, Biomicrofluidics 8 (6) (2014) http://dx.doi.org/10.1063/1.4903948.
[22] Yago Juste-Lanas, Pedro Enrique Guerrero, Daniel Camacho-Gómez, Silvia Hervás-Raluy, Jose M García-Aznar, María J Gomez-Benito, Confined cell migration and asymmetric hydraulic environments to evaluate the metastatic potential of cancer cells, J. Biomech. Eng. 144 (7) (2022) 074502, http://dx.doi.org/10.1115/1.4053143.
[23] Vanesa Olivares, Mar Cóndor, Cristina Del Amo, Jesús Asín, Carlos Borau, José Manuel García-Aznar, Image-based characterization of 3D collagen networks and the effect of embedded cells, Microsc. Microanal. 25 (4) (2019) 971–981.
[24] María Anguiano, Carlos Castilla, Martin Maška, Cristina Ederra, Rafael Peláez, Xabier Morales, Gorka Munoz-Arrieta, Maite Mujika, Michal Kozubek, Arrate Munoz-Barrutia, et al., Characterization of three-dimensional cancer cell migration in mixed collagen-matrigel scaffolds using microfluidics and image analysis, PLoS One 12 (2) (2017) e0171417, http://dx.doi.org/10.1371/journal.pone.0171417.
[25] J Plou, Y Juste-Lanas, V Olivares, C Del Amo, C Borau, JM García-Aznar, From individual to collective 3D cancer dissemination: roles of collagen concentration and TGF-β, Sci. Rep. 8 (1) (2018) 12723.
[26] Ioannis K Zervantonakis, Shannon K Hughes-Alford, Joseph L Charest, John S Condeelis, Frank B Gertler, Roger D Kamm, Three-dimensional microfluidic model for tumor cell intravasation and endothelial barrier function, Proc. Natl. Acad. Sci. 109 (34) (2012) 13515–13520.
[27] Yago Juste-Lanas, Natalia Díaz-Valdivia, Alejandro Llorente, Rafael Ikemori, Alejandro Bernardo, Marselina Arshakyan, Carlos Borau, Josep Ramírez, José Carlos Ruffinelli, Ernest Nadal, et al., 3D collagen migration patterns reveal a SMAD3-dependent and TGF-β1-independent mechanism of recruitment for tumour-associated fibroblasts in lung adenocarcinoma, Brit. J. Cancer 128 (6) (2023) 967–981.
[28] O Moreno-Arotzena, C Borau, N Movilla, M Vicente-Manzanares, JM García-Aznar, Fibroblast migration in 3D is controlled by haptotaxis in a non-muscle myosin II-dependent manner, Ann. Biomed. Eng. 43 (2015) 3025–3039.
[29] Nieves Movilla, C. Borau, C. Valero, J.M. García-Aznar, Degradation of extracellular matrix regulates osteoblast migration: A microfluidic-based study, Bone 107 (2018) 10–17.
[30] Leo Boneschansker, Jun Yan, Elisabeth Wong, David M Briscoe, Daniel Irimia, Microfluidic platform for the quantitative analysis of leukocyte migration signatures, Nat. Commun. 5 (1) (2014) 4787, http://dx.doi.org/10.1038/ncomms5787.
[31] Henry Cavanagh, Daryan Kempe, Jessica K Mazalo, Maté Biro, Robert G Endres, T cell morphodynamics reveal periodic shape oscillations in three-dimensional migration, J. R. Soc. Interface 19 (190) (2022) 20220081.
[32] Luis Saucedo-Mora, Miguel Ángel Sanz, Francisco Javier Montáns, José María Benítez, A simple agent-based hybrid model to simulate the biophysics of glioblastoma multiforme cells and the concomitant evolution of the oxygen field, Comput. Methods Programs Biomed. 246 (2024) 108046, http://dx.doi.org/10.1016/j.cmpb.2024.108046.
[33] Inês G. Gonçalves, Jose Manuel Garcia-Aznar, Extracellular matrix density regulates the formation of tumour spheroids through cell migration, PLoS Comput. Biol. 17 (2) (2021) e1008764, http://dx.doi.org/10.1371/journal.pcbi.1008764.
[34] Gabriella Bretti, Andrea De Gaetano, An agent-based interpretation of leukocyte chemotaxis in cancer-on-chip experiments, Mathematics 10 (8) (2022) 1338, http://dx.doi.org/10.3390/math10081338.
[35] Qiyao Peng, Fred J. Vermolen, Daphne Weihs, Physical confinement and cell proximity increase cell migration rates and invasiveness: A mathematical model of cancer cell invasion through flexible channels, J. Mech. Behav. Biomed. Mater. 142 (2023) 105843, http://dx.doi.org/10.1016/j.jmbbm.2023.105843.

[36] Clara Valero, Hippolyte Amaveda, Mario Mora, Jose Manuel García-Aznar, Combined experimental and computational characterization of crosslinked collagen-based hydrogels, PLoS One 13 (4) (2018) e0195820, http://dx.doi.org/10.1371/journal.pone.0195820.

[37] Nieves Movilla, Inês G Gonçalves, Carlos Borau, Jose Manuel García-Aznar, A novel integrated experimental and computational approach to unravel fibroblast motility in response to chemical gradients in 3D collagen matrices, Integr. Biol. 14 (8–12) (2022) 212–227, http://dx.doi.org/10.1093/intbio/zyad002.

[38] David M Davies, Julie Foster, Sjoukje JC Van Der Stegen, Ana C Parente-Pereira, Laura Chiapero-Stanke, George J Delinassios, Sophie E Burbridge, Vincent Kao, Zhe Liu, Leticia Bosshard-Carter, et al., Flexible targeting of ErbB dimers that drive tumorigenesis by using genetically engineered T cells, Mol. Med. 18 (4) (2012) 565–576, http://dx.doi.org/10.2119/molmed.2011.00493.

[39] Hongxia Li, Emily B Harrison, Huizhong Li, Koichi Hirabayashi, Jing Chen, Qi-Xiang Li, Jared Gunn, Jared Weiss, Barbara Savoldo, Joel S Parker, et al., Targeting brain lesions of non-small cell lung cancer by enhancing CCL2-mediated CAR-T cell migration, Nature Commun. 13 (1) (2022) 2154, http://dx.doi.org/10.1038/s41467-022-29647-0.

[40] Philip Lee, Rob Lin, James Moon, Luke P. Lee, Microfluidic alignment of collagen fibers for in vitro cell culture, Biomed. Microdev. 8 (2006) 35–41, http://dx.doi.org/10.1007/s10544-006-6380-z.

[41] Adeel Ahmed, Indranil M Joshi, Madeleine R Goulet, Justin A Vidas, Ann M Byerley, Mehran Mansouri, Steven W Day, Vinay V Abhyankar, Microengineering 3D collagen hydrogels with long-range fiber alignment, JoVE (J. Vis. Exp.) (187) (2022) e64457, http://dx.doi.org/10.3791/64457.

[42] Cristina Del Amo, Vanesa Olivares, Mar Cóndor, Alejandro Blanco, Jorge Santolaria, Jesús Asín, Carlos Borau, José Manuel García-Aznar, Matrix architecture plays a pivotal role in 3D osteoblast migration: The effect of interstitial fluid flow, J. Mech. Behav. Biomed. Mater. 83 (2018) 52–62, http://dx.doi.org/10.1016/j.jmbbm.2018.04.007.

[43] Johannes Huth, Malte Buchholz, Johann M Kraus, Kristian Mø lhave, Cristian Gradinaru, Götz v Wichert, Thomas M Gress, Heiko Neumann, Hans A Kestler, TimeLapseAnalyzer: multi-target analysis for live-cell imaging and time-lapse microscopy, Comput. Methods Programs Biomed. 104 (2) (2011) 227–234, http://dx.doi.org/10.1016/j.cmpb.2011.06.002.

[44] Ângela Carvalho, Tiago Esteves, Pedro Quelhas, Fernando Jorge Monteiro, MobilityAnalyser: A novel approach for automatic quantification of cell mobility on periodic patterned substrates using brightfield microscopy images, Comput. Methods Programs Biomed. 162 (2018) 61–67, http://dx.doi.org/10.1016/j.cmpb.2018.05.003.